Noname manuscript No.
(will be inserted by the editor)

JYFLTRAP: a Penning trap for precision mass spectroscopy and isobaric purification

T. Eronen · V.S. Kolhinen · V.-V. Elomaa · D. Gorelov · U. Hager · J. Hakala · A. Jokinen · A. Kankainen · P. Karvonen · S. Kopecky · I.D. Moore · H. Penttilä · S. Rahaman · S. Rinta-Antila · J. Rissanen · A. Saastamoinen · J. Szerypo · C. Weber · J. Äystö ·

Received: date / Accepted: date

Abstract In this article a comprehensive description and performance of the double Penning trap setup JYFLTRAP will be detailed. The setup is designed for atomic mass measurements of both radioactive and stable ions and additionally serves as a very high resolution mass separator. The setup is coupled to the IGISOL facility at the accelerator laboratory of the University of Jyväskylä. The trap has been online since 2003 and it was shut down in summer 2010 for relocation to upgraded IGISOL facility. Numerous atomic mass and decay energy measurements have been performed using the time-of-flight ion-cyclotron resonance technique. Also the trap has been used in several decay spectroscopy experiments as a high-resolution mass filter.

Keywords Penning trap · atomic mass measurement · Q-value measurement · isobaric purification

T. Eronen · V.S. Kolhinen · V.-V. Elomaa · D. Gorelov · U. Hager · J. Hakala · A. Jokinen · A. Kankainen · P. Karvonen · S. Kopecky · I.D. Moore · H. Penttilä · S. Rahaman · S. Rinta-Antila · J. Rissanen · A. Saastamoinen · J. Szerypo · C. Weber · J. Äystö ·
P.O. Box 35 (YFL), 40014 University of Jyväskylä, Finland
E-mail: tommi.eronen@jyu.fi
Present addresses:
T. Eronen: Max-Planck-Institut für Kernphysik, Saupfercheckweg 1, 69117 Heidelberg, Germany
V.-V. Elomaa: Turku PET Centre, Accelerator Laboratory, Åbo Akademi University, 20500 Turku, Finland
U. Hager: Colorado School of Mines, Golden, CO, USA
S. Kopecky: European Commission - Joint Research Centre, Institute for Reference Materials and Measurements, Retieseweg 11, B-2440 Geel
S. Rahaman: Los Alamos National Laboratory, Los Alamos, NM 87545, USA
J. Szerypo, C. Weber: Fakultät für Physik, LMU München and Maier-Leibnitz Laboratory, Am Coulombwall 1, 85748 Garching, Germany

1 Introduction

Ion manipulation and trapping techniques have opened a new powerful way to study ground state properties of stable and of short-living ions. Penning trap mass spectrometry has become a routine technique for high-precision mass measurements and one can measure atomic masses of stable ions with a relative uncertainty $\delta m/m < 10^{-10}$ and short-living ions with $\delta m/m < 10^{-8}$ [1]. Uncertainties of this level allows to investigate many physics phenomena through atomic mass [2].

Stable-ion traps such as SMILETRAP in Stockholm [3], the trap setup at Florida state University [4] and the University of Washington Mass spectrometer (now at Max-Planck-Institute for nuclear physics in Heidelberg, Germany) [5,6] have measured several masses of stable nuclei with precision of better than 10^{-10}. Some of the high-precision results are actually used as reference masses for on-line Penning trap setups. Also, Penning traps for anti-matter studies (e.g. ATRAP [7] and ASACUSA [8]) have performed high precision mass measurements of anti-matter ions.

Most of the radioactive ion beam facilities that can provide beams of short-living ions have implemented a trap to be a part of their setup. Presently there are several functioning traps around the world which perform mass measurements with radioactive ions like CPT in ANL [9], ISOLTRAP at CERN [10], LEBIT at MSU [11], MLLTRAP at LMU [12], SHIPTRAP at GSI [13], TITAN at TRIUMF [14], TRIGATRAP at the Mainz research reactor [15] and JYFLTRAP at the University of Jyväskylä [16, 17]. These so-called on-line traps are typically very fast (can access nuclei with short half-lives; see e.g. [18]) and also efficient in terms of very low production rate (see e.g. [19]).

In this article the JYFLTRAP double Penning trap setup will be described in detail. In short, the setup is designed to perform high-resolution beam purification and mass measurements with both stable and radioactive ion beams created with the Ion Guide Isotope Separator On-Line (IGISOL) technique [20, 21].

2 Basic Principles

2.1 Ion beam production and separation

The JYFLTRAP setup receives beams from IGISOL, which is extensively discussed elsewhere in this IGISOL portrait volume. The radioactive ions created either by fission or fusion reactions are stopped in helium gas, extracted by using electric fields and a helium gas jet via a sextupole ion guide (SPIG) [22], and are finally electrostatically accelerated to $30q$ keV of energy, where q is the charge state of ions (usually $q = 1$). Alternatively, an electric discharge ion source can be used to create ions of stable isotopes (see *e.g.* Ref. [23] for more details). The extracted ion beam is mass-separated with a 55° dipole magnet (see Fig. 1) allowing for a mass resolving power ($M/\Delta M$) of about 500.

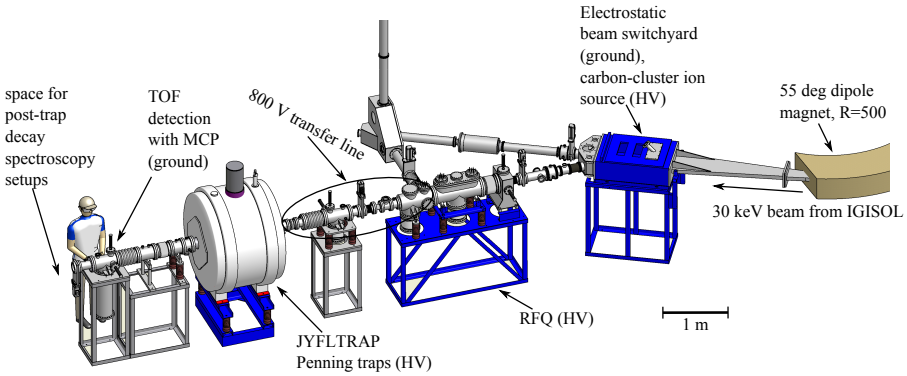

Fig. 1 The experimental area of the IGISOL facility which is mostly occupied by the radiofrequency quadrupole (RFQ) cooler-buncher and the JYFLTRAP Penning trap setup. Devices operated in high voltage are marked with (HV). The 30-keV ion beam from IGISOL (incident from right) is mass-separated with a 55° dipole magnet and deflected with an electrostatic 30° deflector to left towards the RFQ and JYFLTRAP setups. The setup is described in detail in section 3.

2.2 Radiofrequency quadrupole cooler-buncher

The mass-separated ion beam from IGISOL is injected into a radiofrequency quadrupole cooler-buncher (RFQ) [24]. The $30q$ keV ion beam is electrostatically decelerated to ∼100 eV of energy by having the whole RFQ on a high voltage (HV) platform. The decelerated beam then enters inside the quadrupole rod structure filled with helium buffer gas at low pressure. The ions are cooled by collisions with buffer gas atoms and collected in a potential well. The cooled ions are periodically released to the Penning traps as short, 10–15μs, bunches.

2.3 Principle of a Penning trap

In general, a Penning trap is a device to confine charged particles to a small volume with a static quadrupolar electric field and a homogeneous magnetic field. The electric potential in cylindrical coordinates (z, ρ) is of the form

$$V(z,\rho) = \frac{U_0}{4d^2}\left(2z^2 - \rho^2\right), \tag{1}$$

where U_0 is the potential difference between the ring and endcap electrodes and $d = \sqrt{2z_0^2 + r_0^2}$ is the characteristic trap parameter defined by the trap geometry: $2z_0$ is the distance between endcap electrodes and r_0 is the inner radius of the ring electrode.

The trapped charged particles exhibit three different eigenmotions. One of the motions, called the axial motion with frequency ν_z, occurs along the magnetic field lines. The other two motions are in a plane perpendicular to the magnetic field and are commonly called radial motions. These can be distinguished by their frequencies ν_- and ν_+. The magnetron motion with the

lower frequency ν_- is almost mass independent. The second motion described by the reduced cyclotron frequency ν_+, exhibits a mass dependence, and the sum of the two frequencies is given by the cyclotron frequency ν_c:

$$\nu_- + \nu_+ = \nu_c = \frac{1}{2\pi}\frac{q}{m}B, \tag{2}$$

where q and m are the charge and mass of the ion, respectively, and B the magnetic field. For an ion with $A/q = 100$ trapped in a 7 T magnetic field via a Penning trap (potential depth of the order of 100 V), the reduced cyclotron frequency, the magnetron frequency, and the axial oscillation frequency are of the order of $\nu_+ \approx 1$ MHz, $\nu_- \approx 2$ kHz, and $\nu_z \approx 50$ kHz. It should be noted that Eq. (2) is only valid in an ideal case where the quadrupolar electric field is fully harmonic and the magnetic field perfectly homogeneous. In the case of a real Penning trap a more robust relationship is the invariance theorem [25,26]

$$\nu_c^2 = \nu_-^2 + \nu_+^2 + \nu_z^2. \tag{3}$$

In Fig. 2 the three eigenmotions in a Penning trap are illustrated.

One important aspect of many on-line Penning traps such as ISOLTRAP, SHIPTRAP, MLLTRAP and JYFLTRAP is ion motion damping in a gas-filled trap. Introducing buffer-gas into the Penning trap will lead to a modification of the ion's motion [27]. The interaction between the gas and the ions will decrease the oscillation amplitude in the axial direction and reduce the radius of the modified cyclotron motion. However, the radius of the magnetron motion will increase.

2.4 Excitation of the ion motion in a Penning trap

The operation principle of a Penning trap is based on the manipulation of the trap eigenmotions. This is achieved by applying RF signals to different trap electrodes. In the case of JYFLTRAP, the ring electrodes are eight-fold segmented for exciting the radial eigenmotions. The effect of these excitations to the motion of trapped ions depends on the excitation mode and the applied parameters: the frequency, the amplitude, the duration and the envelope of the RF field. At JYFLTRAP, the RF electric fields are applied either in a dipolar or in a quadrupolar mode.

In the dipolar excitation the frequency is applied to the two opposite segments of the central ring electrode in such a way that the segments have the same frequency and amplitude, but opposite phase. At JYFLTRAP, a simplified excitation scheme is used, where the RF signal is fed only to one quadrant (two neighboring octants) of the ring electrode, while applying a static voltage to the others. Dipolar excitations at eigenfrequencies can be used to excite one particular eigenmotion without affecting the other two. Typically, the dipolar excitation is applied at the mass independent magnetron frequency ν_- or at the mass dependent reduced cyclotron frequency ν_+ to enlarge the radius of the corresponding motion, i.e., to move ions away from the trap center.

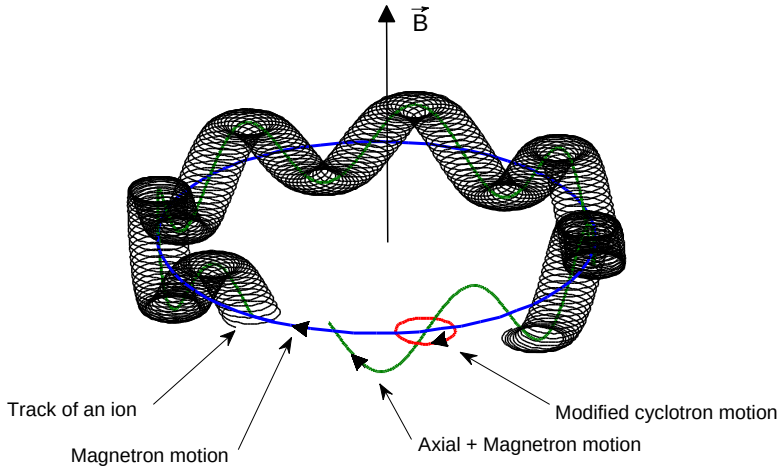

Fig. 2 (color online) Motion of a positively charged ion in a Penning trap with magnetic field lines pointing up. Figure shows a track of an ion having component of all three motions. The blue and red lines show motion of an ion having only magnetron or reduced cyclotron motion, respectively, while the green track is for an ion with both magnetron and axial motion. The frequencies are not to scale.

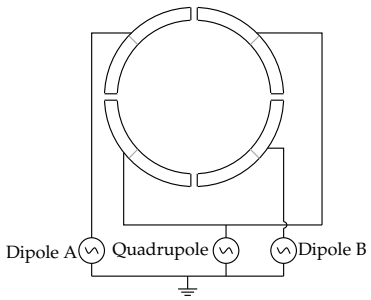

Fig. 3 The four-fold split ring electrode (top view). Each quadrant is formed by interconnecting two octants. At JYFLTRAP, two of the quadrants are used for quadrupole excitation and the two other for dipolar excitations: Dipole A for magnetron (ν_-) and Dipole B for modified cyclotron (ν_+) motion excitation.

A quadrupolar excitation can be achieved by using four segments and applying voltages in such a way that opposite segments receive the same frequency, amplitude and phase, while the two other segments, that are in a 90° angle relative to two first ones, receive the same frequency and amplitude but the opposite phase. Here also a simplified excitation scheme is used at JYFLTRAP by connecting two opposite quadrants (two octants) to the same RF signal, while applying a static voltage to the two other quadrants. This quadrupolar type excitation is usually called as a side-band excitation. When one applies quadrupolar excitation with the mass dependent cyclotron frequency $\nu_{\mathrm{RF}} = \nu_c = \frac{1}{2\pi}\frac{q}{m}B$ the two radial eigenmotions are bound together and there is a continuous conversion from one motion to the other. Figure 3 illustrates the connections of the ring electrode during dipolar and quadrupolar excitations. A more detailed description of the operation principles of a Penning trap can be found for example in Ref. [28].

2.5 Time-of-flight ion-cyclotron resonance technique

At JYFLTRAP, the cyclotron frequency (ν_c) is determined with the time-of-flight ion-cyclotron resonance (TOF-ICR) technique [29, 30] which is based on probing the cyclotron frequency in the trap and measuring the flight time of the ions from the trap to a microchannel plate (MCP) detector which is located outside the strong magnetic field, see Fig. 1. This technique provides a universal and fast way to perform mass measurements with a relatively low number of ions.

Initially, a small number of ions (ideally just one since larger number induces frequency shifts due to their mutual interaction) is injected into the trap. Next a dipolar excitation with the magnetron frequency ν_- is applied which leads to an increased magnetron orbit of all ions. Subsequently quadrupolar excitation is then used to mass-selectively convert the magnetron motion into modified cyclotron motion. Due to this conversion from the low-frequency

magnetron motion to the high-frequency modified cyclotron motion (the difference in the frequency can be as large as 10^5), the radial energy E_r of the ions will be increased. Larger radial energy leads to stronger axial acceleration of ions in the gradient of the magnetic field after the extraction according to the equation

$$\mathbf{F} = -\boldsymbol{\mu}(\boldsymbol{\nabla} \cdot \mathbf{B}) = -\frac{E_r}{B_0}\frac{\partial B(z)}{\partial z}\hat{z}, \tag{4}$$

where $\boldsymbol{\mu} = (E_r/B_0)\hat{z}$ is the magnetic moment of the ion; B_0 is the magnetic field at precision trap and E_r radial energy of the ion. The measurement procedure is then done by scanning the quadrupolar excitation frequency ν_{RF} around the cyclotron frequency ν_{c} and determining the frequency resulting in the shortest flight time from the trap to the MCP detector. The flight time can be calculated by using the formula

$$T(\omega) = \int_0^{z'} \sqrt{\frac{m}{2(E_0 - qU(z) - \mu B(z))}}dz, \tag{5}$$

where E_0 is the initial axial kinetic energy of the ion, $U(z)$ is the electrostatic potential and $B(z)$ is the magnetic field along the flight path [30]. Figure 4 shows a typical TOF-ICR spectrum. The conversion from magnetron motion to modified cyclotron motion is periodic and the conversion rate depends on the excitation time T_{RF} and the amplitude U_{RF}. To achieve full conversion after the excitation in resonance the values T_{RF} and U_{RF} must be carefully chosen. Once the values are experimentally found, their product is kept constant:

$$T_{RF}U_{RF} = \text{const.} \tag{6}$$

The value of this constant depends of the trap geometry (see Eq. 1) and has been experimentally determined to be 11.2 mVs for JYFLTRAP. This full conversion happens only at the frequency $\nu_{RF} = \nu_c = \nu_+ + \nu_-$. At other frequencies the conversion is only partial. The line width of the resonance is inversely proportional to the excitation time T_{RF}, i.e., longer excitation time gives better mass resolving power.

2.5.1 Excitation with time-separated oscillatory fields

Excitation with time-separated oscillatory fields was introduced by N.F. Ramsey [31] and first time demonstrated to Penning trap mass spectrometry at ISOLTRAP [32]. Once the analytical form for the spectrum shape became available [33, 34], this method has been routinely used in many trap facilities. Typically the time-separated oscillatory fields method is performed with two equally long RF-on periods interrupted with a certain time duration. It is important to retain phase coherence for the two RF-on periods. With same statistics typically a factor of 2 to 3 better precision is obtained than with the conventional cyclotron frequency determination described in the previous. The main peak is 40% narrower but most of the enhancement is due to fact that more frequency scan points lie on high-slope parts of the curve than in

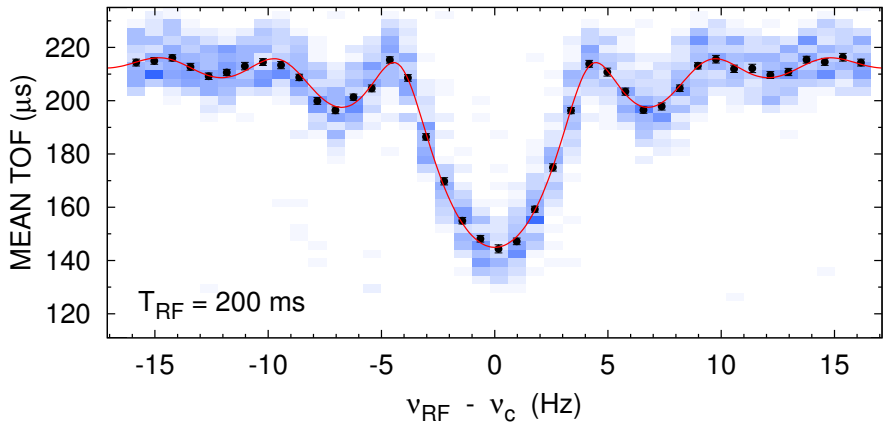

Fig. 4 A time-of-flight ion-cyclotron resonance curve for $^{54}Co^{+}$ ions ($T_{1/2} \approx 200$ ms). An excitation time T_{RF} of 200 ms was used. The pixels represent detected ions; the shading is proportional to the number of detected ions.

the conventional resonance. Typically the quadrupole RF field is switched on for 20-50 ms, then off for 150-750 ms (mostly depending on the half-life of the ion of interest), and finally switched on for another 20-50 ms. Naturally, any excitation scheme must fulfill Eq. 6 for "RF-on" periods in order for ions to undergo one full conversion from magnetron to modified cyclotron motion. A typical TOF-ICR curve obtained with time-separated oscillatory fields technique is shown in Fig. 5. In order to unambiguously assign the center fringe corresponding to ν_c a conventional TOF-ICR curve can be recorded.

One important application employing ion motion excitation with time-separated oscillatory fields is the so-called "Ramsey cleaning technique" [35] which is used in high-resolution mass separation. This method has been developed at JYFLTRAP and is described in detail in section 5.1.

3 The JYFLTRAP experimental setup

The JYFLTRAP consists of two Penning traps located inside the same superconducting solenoid. The ions are injected from the RFQ (see Ref. [24] for more details). The RFQ cooler-buncher and JYFLTRAP are on a single 30 kV high voltage platform. This way, the ion beam incident from IGISOL can be electrostatically slowed down. The ion bunches from the RFQ are ideal to be injected into the JYFLTRAP setup: they have energy and temporal spreads of less than 1 eV and 15 μs, respectively. The JYFLTRAP setup is shown in Fig. 1. Marked with HV are the devices that are operated on a high-voltage platform. The ions are transferred from the RFQ to the Penning traps as an 800 eV ion beam. In the following subsections technical details of the JYFLTRAP setup are given.

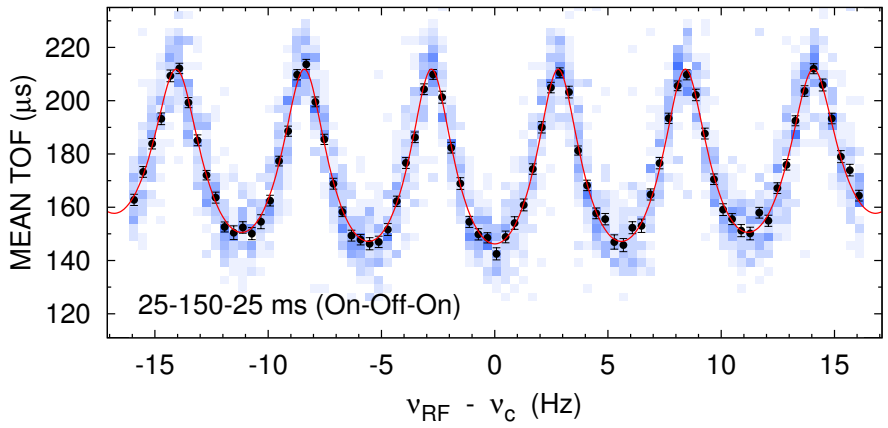

Fig. 5 A time-of-flight ion-cyclotron resonance curve for $^{54}Co^{+}$ ions ($T_{1/2} \approx 200$ ms) obtained with Ramsey's method of time-separated oscillatory fields. An excitation time pattern of 25-150-25 ms (On-Off-On) was used. It should be noted that this figure has twice the amount of scanned frequency points than Fig. 4.

3.1 Superconducting magnet

The most visible part of the JYFLTRAP setup is the superconducting magnet that creates the magnetic field of the Penning traps. It is an actively screened 7.0-T superconducting solenoid manufactured by Magnex Scientific Ltd. in the UK. The magnet has a 160-mm-diameter warm bore. The generated field is fine-tuned both with superconducting shimming coils and with ferromagnetic metal strips placed around the bore tube in order to create two homogeneous 1 cm^3 field regions 10 cm apart from the center of the magnet. The relative homogeneity of the magnetic field ($\Delta B/B$) has been ≈ 0.4 ppm in both traps after restarting the magnet in 2007. The superconducting solenoid is placed on a high-voltage platform along with all the trap electronics.

The stainless steel (grade 316L) vacuum tube inside the bore is mounted with adjustable fasteners allowing alignment of the beam tube with respect to the magnetic field axis. The alignment was performed by inserting an electron source to the center of the magnet and guiding the two beams of electrons following the magnetic field lines through a set of narrow collimators placed on both sides of the trap center. The same alignment procedure was later adapted also at MLLTRAP and details of the alignment procedure can be found in Ref. [12].

3.2 Trap structure

All vacuum chambers are built of grade 316L non-magnetic stainless steel using the con-flat (CF) flange standard. Two turbomolecular pumps of 880 l/s are

located at the injection and at the extraction side of the magnet. The pressure in the vacuum volume of the Penning traps (without any gas load) is well below the lower limit of the Penning pressure gauge (5×10^{-9} mbar).

All electrodes not within the superconducting solenoid are made of either aluminium or of stainless steel. The electrodes within the solenoid forming the trap electric field are made of gold plated oxygen-free copper and they are electrically isolated from each other by aluminium-oxide insulators. In total about 50 gold-plated copper electrodes form a 1046-mm-long electrode structure, see Fig. 6. For ease of assembly, the electrodes are subdivided to seven segments held together with aluminium rods. Once the segments are interconnected the whole package can be inserted into the vacuum tube as one unit from the extraction side. All trap electrodes are cylindrical. These are much easier to manufacture than hyperbolic electrodes and also better vacuum can be achieved in the precision trap due to open geometry. Most of the electrodes have an inner diameter of 32 mm.

Each of the two cylindrical Penning traps of JYFLTRAP (see Fig. 6) consist of an 8-fold split ring electrode (A), two-fold splitted inner correction electrodes (B) on each side of the ring electrode, outer correction electrodes (C) and endcap electrodes (D) located next to the correction electrodes. The dimensions of the electrodes have been scaled from the ISOLTRAP purification trap [36–38]. The lengths of the ring electrode, the first and the second correction electrode and the endcap electrode are 18.5, 12.8, 6.7 and 44 mm, respectively, separated by 0.5 mm. The trap nearest to the RFQ is called the purification trap and is filled with dilute helium gas to enable the use of buffer-gas cooling of ions (see Sec. 4 for more explanation). Gas flow to other sections of the system is minimized with the use of electrodes having narrow channels (see Fig. 6 electrodes E and F). The other trap, commonly referred as the precision trap is located on the extraction side, 20 cm away from the purification trap center.

Table 1 shows the typical voltages used in the injection section of the trap. Tables 2 and 3 show the dimensions of the trap electrodes and trapping and extraction voltages applied in the purification and precision traps, respectively. The extraction side voltages when the trap is used for atomic mass measurements are given in table 4. When ions are extracted to the post-trap decay spectroscopy station, the voltages are somewhat different to optimally transfer ions further out from the trap setup.

The voltages to the trap electrodes are fed into the vacuum tube on both sides of the solenoid with so-called plug chambers. Each plug chamber houses three 500-V 10-pin feedthroughs connected via silver-plated copper wires into 30 evenly distributed sockets on the circumference of an insulating ring made of PEEK. At the ends of the trap structure there are similar rings with pins that fit into the sockets of the plug chambers. The trap electrodes are connected to the pins via silver-plated copper leads. This structure allows for a relatively fast way to insert the trap structure into the vacuum tube and to connect the electrical contacts.

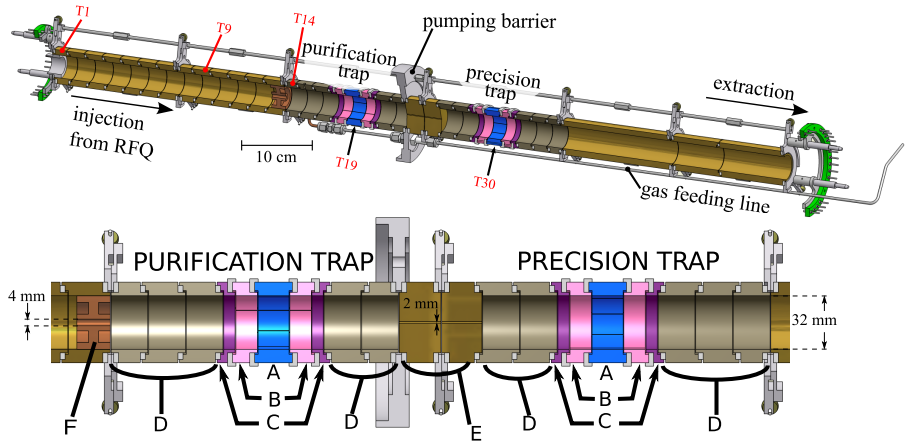

Fig. 6 (color online) The electrodes inside the superconducting magnet forming the JYFLTRAP double Penning trap. The center of the trap is expanded for clarity. The 8-fold split ring electrodes are marked with A, the two-fold split inner correction electrodes with B, outer correction electrodes with C and the endcap electrodes with D. For reference, the trap electrodes are indexed from left to right with T1,T2, and so on. The ring electrodes are marked T19 and T30. The electrodes restricting the gas flow out are marked with E and F; their inner diameters are 2 mm and 4 mm, respectively.

Electrode	Voltage (V)	Beam energy (qeV)
Transfer section	−800	834
Injection 1	−800	834
Injection 2	−390	423
Injection 3	−350	384
T1-T10	−340	374
T11-T12	−30	64

Table 1 Typical voltages used at the injection ion optics and at the injection section of the trap. Voltages are given with respect to the purification trap ring electrode potential. Transfer section refers to the beam line section between RFQ and trap and Injection 1…3 to three cylindrical electrodes in front of the first trap electrode T1. See also Table 2.

3.3 Electronic devices

The electronic devices required to operate the Penning traps include DC power supplies, high voltage switches and arbitrary waveform generators. In addition, a pulse pattern generator is used to generate 5 V *ON* and *OFF* TTL signals for the switches, waveform generators and other equipment requiring time-dependent operation.

3.3.1 Power supplies

DC power supplies from two manufacturers, ISEG Spezialelektronik GmbH and Spellman High Voltage Electronics Corporation, are used. The ISEG power supplies used in the setup are modular units having their own control electronics with 16 independent outputs and with a voltage range 0 – -500

Electrode	Description	L (mm)	trapping (V)	inj. (V)	extr. (V)
T13	diaphragm (d=4 mm)	24	+100	−20	
T14	gas feeding endcap	21.5	+100	−20	
T15	endcap	22	+100	−20	
T16	endcap	22	+100	+30	
T17	correction 2	6.7	+66	+20	
T18	correction 1	12.8	+17	+20	
T19	ring	18.5	0	0	0
T20	correction 1	12.8	+17		−1
T21	correction 2	6.7	+66		−5
T22	endcap	22	+100		−5
T23	endcap	22	+100		−5
T24	diaphragm (d=2 mm)	24.5	+100		−5

Table 2 Axial lengths of the electrodes in the purification trap (in addition, there is 0.5 mm gap between each electrode) together with the operating voltages for the three modes of operation. The "trapping" denotes voltages used when the ions are stored in the trap and "inj." and "extr." when ions are being injected or extracted from the trap, respectively. The potentials are given with respect to the ring electrode potential. See Fig. 6 for positions of the electrodes.

Electrode	Description	L (mm)	trapping (V)	inj. (V)	extr. (V)
T25	diaphragm (d=2 mm)	24.5	+10	−10	
T26	endcap	22	+10	−10	
T27	endcap	22	+10	−10	
T28	correction 2	6.7	+6.6	−10	
T29	correction 1	12.8	+1.7	−10	
T30	ring	18.5	0	0	0
T31	correction 1	12.8	+1.7		−1
T32	correction 2	6.7	+6.6		−1
T33	endcap	22	+10		−1
T34	endcap	22	+10		−1
T35	endcap	22	+10		−1

Table 3 Axial lengths of the electrodes in the precision trap (in addition, there is 0.5 mm gap between each electrode) together with the operating voltages for three modes of operation. The "trapping" denotes voltages used when ions are stored in the trap and "inj." and "extr." when ions are being injected or extracted from the trap, respectively. The potentials are given with respect to the ring electrode potential. It should be noted that the potential of the precision trap ring electrode is 4.2 V higher than the potential of the purification trap ring electrode. See Fig. 6 for positions of the electrodes.

V. All electrodes listed in Tables 1, 2, 3, and 4 having voltages less than 500 V are connected to these units. The ISEG modules have better voltage stability than the Spellman ones. Other electrodes requiring more than 500 V are connected to Spellman power supplies. Each of these power supplies have one output whose output level is determined by a 0 – 10 V control signal. These control signals are provided by digital-to-analog (DAC) modules in modular I/O systems manufactured by WAGO Kontakttechnik GmbH & Co. The ISEG crate and WAGO I/O systems are connected to a computer by a Control Area Network (CAN) fieldbus via fiber optic repeaters.

Electrode	Voltage (V)
T36	−2
T37	−3
T38	−4
plug chamber el.	−100
extraction 1	−150
extraction 2	−1200
Shield grid	−900
Einzel 1	+8000
(Einzel 2	+2500)

Table 4 Typical voltages used at the extraction section of the trap. The electrode voltages above the single horizontal line are given with respect to the precision trap ring electrode. After "extraction 2" electrode the ions are accelerated to $30q$ keV. The voltages below the single horizontal line are given with respect to groud potential.

Manufacturer	Model	Outputs	V_{min} (V)	V_{max} (kV)	I_{max} (mA)
ISEG	EHQ F005n	16	0	-0.5	0.25
Spellman	MP5N	1	0	-5	2.0
Spellman	MP10N	1	0	-10	1.0
Spellman	MP5P	1	0	5	2.0
Spellman	MP20P	1	0	20	0.5
Spellman	MP40P	1	0	40	0.2

Table 5 Summary of the DC power supply modules in use.

3.3.2 High voltage switches

Ion samples are either injected to, trapped in or extracted from the purification or precision trap by switching the voltages of electrodes from "injection" or "extraction" to "trapping" voltage levels or vice versa. For each switchable electrode two voltage outputs from the ISEG power supply are connected to a high voltage switch. One ISEG output may supply voltage to multiple electrodes as shown in Tables 2 and 3, for example to the electrodes from T13 to T15 in "open" mode. The switches are controlled by TTL signals.

Two kinds of high voltage switches have been used, one for the 100-V-deep purification trap and one for the 10-V-deep precision trap. The switch for the purification trap is based on a Supertex inc. HV20822 16-channel high voltage analog switch integrated circuit, which has two sets of eight analog switches and two corresponding digital inputs for TTL signals. The switch for the precision trap has been designed using UC2707 dual channel power drivers for switching and HFBR-2524 fiber optical receivers to control switching. OPA445 precision amplifiers have been used to boost the low current outputs from the ISEG power supplies.

3.3.3 Arbitrary waveform generators

The segmented ring electrodes of the two traps are connected to arbitrary waveform generators through AC/DC coupling boxes consisting of one resistor and a capacitor. Three models manufactured by Agilent Technologies are in

use: 31120A, 31220A and 33250A (see Table 6). The major difference between these models is the maximum frequency in *continuous* and so-called *burst start* mode. A LAN/GPIB gateway made by Agilent Technologies is used to connect the waveform generators to a computer via Ethernet. A pair of Ethernet media converters bridges the high voltage platform and the ground via a pair of fiber optic cables.

Model	Maximum frequency (MHz)		Connectivity
	continuous	*burst start*	
33120A	15	5	GPIB, RS232
33220A	20	6	GPIB, Ethernet
33250A	80	25	GPIB, RS232

ID	Trap	Type	Motion	Model	Mode	Remark
RF1	1	Dipole	ν_-	33120A	*burst start*	
RF2	1	Quadrupole	ν_c	33250A	*gated*	
RF3	2	Dipole	ν_-	33220A	*burst start*	
RF4	2	Quadrupole	ν_c	33250A	*gated*	Fixed starting phase
					AM	Ramsey excitation
RF5	2	Dipole	ν_+	33120A	*gated*	Ramsey cleaning
RF6	2	AM		33120A	*burst start*	AM of RF4

Table 6 Arbitrary waveform generators and their usage.

Arbitrary waveform generators have a connector for a TTL input signal that can be used in two ways. In *burst start* mode the TTL signal determines when the generator outputs a predefined number of (sine) waveforms, for example 17 periods of sine waveform with ν=1.7 kHz suitable for the 10 ms long magnetron excitation in the purification trap. In *gated* mode the generator repeats a (sine) waveform as long as the TTL signal remains in the *ON* level. In addition, amplitude modulation (*AM*) used with Ramsey-type of excitation is possible via a separate input terminal. In this mode the starting phase of the excitation waveform is random but the phase is continuous for the excitation periods [39].

3.3.4 Pulse pattern generator

The high voltage switches and RF generators require precise timing signals. A PCI-card named PulseBlaster (model PB24-32k) is installed to a computer in order to provide these TTL signals for timings. It has 24 output channels and a 100 MHz clock which translates to a pulse resolution of 10 ns. The program executed by the card can contain up to 32,768 instructions that can last from 90 ns to 1.4 years each.

Most of the outputs from the card are connected to fiber optic transmitters through a buffer circuit. At the other end of each fiber optic cable is a fiber optic receiver which provides TTL signals for example to a high voltage switch or to an arbitrary waveform generator.

3.3.5 Time-of-flight measurement

The signal of the amplifier of the MCP detector is recorded by a Multichannel Scaler/Averager (MCS) – Model SR430 – that is made by Stanford Research System. It has a built-in discriminator with a typical pulse pair resolution of 10 ns. In the most common scenario, the recording time is 1024 times the 0.64 μs bin width. A TTL timing signal from the pulse pattern generator signals the device when to start counting ions as a function of time. The MCS is connected to a computer via GPIB bus and a LAN/GPIB gateway.

4 Purification trap

The first of the JYFLTRAP Penning traps is called the purification trap. It is filled with helium gas and is used for isobaric purification of ion beam. Trapped ions are manipulated by applying multipole RF fields to the azimuthally split ring electrode. After an initial cooling period without excitation, an azimuthal dipole field with magnetron frequency ν_- is switched on for a short duration ($\approx$10 ms). This inreases the magnetron radius of all ions. The amplitude of the RF field is chosen so that no ion, upon extraction, can pass through the narrow channel of electrode E shown in Fig. 6. After the azimuthal dipolar excitation, a quadrupole RF field with the cyclotron frequency of the ion of interest (see Eq. 2) is switched on. This excitation causes conversion from magnetron motion to modified cyclotron motion. Due to this, amplitudes of both the magnetron motion starts to decrease and also the modified cyclotron motion decreases in the presence of buffer gas, which will center the ions of interest in the trap. Therefore, a mass-selected beam can be extracted through a diaphragm out of the purification trap. The mass resolving power of the purification depends on the physical dimension of the diaphragm, on the buffer gas pressure and the amplitudes of the applied fields. At JYFLTRAP, a mass resolving power $M/\Delta M$ of the order of 10^5 has been achieved, see Fig. 7. More details are given in Ref. [16].

5 Precision trap

The precision trap is geometrically almost identical to the purification trap. It is primarily used for high-precision atomic mass measurements employing time-of-flight ion-cyclotron resonance (TOF-ICR) technique [29, 30], and secondarily for high-resolution beam purification [35] reaching a mass resolving power of 10^6 or more.

5.1 High-resolution beam purification

If the mass resolving power of the purification trap is not sufficient to prepare monoisobaric (or monoisomeric) ion samples, the precision trap can be utilized

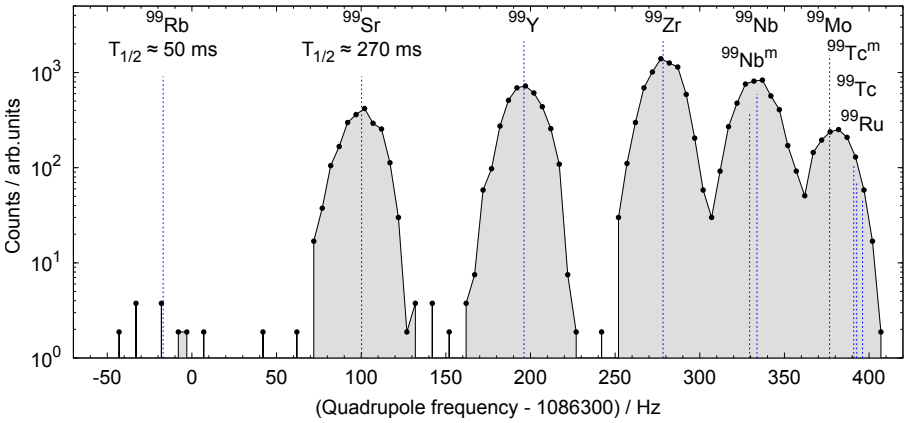

Fig. 7 Quadrupole frequency scan in the purification trap for ions produced in proton-induced fission at $A = 99$. Cyclotron resonance frequencies ν_c for various products have been labeled and marked with dashed vertical lines. The isotopes and isomers close to the stable ^{99}Ru are not fully resolved. A full-width at half-maximum ($\Delta\nu_{\mathrm{FWHM}}$) of 30 Hz is obtained, corresponding to a mass resolving power $M/\Delta M \approx 30{,}000$.

to provide even better mass resolution. Typically $\Delta\nu_{\mathrm{FWHM}}$ of 10...20 Hz (or slightly better with reduced transmission) can be reached with the purification trap. Here we give a brief description of a high-resolution cleaning method employing both the purification and the precision trap providing even better than ∼1 Hz resolution. A more comprehensive discussion of this so-called "Ramsey cleaning method" is given in Ref. [35].

The high-resolution cleaning is performed only after the pre-purification with the purification trap. The pre-cleaned bunch of ions is captured to the precision trap where contaminant ions are excited to larger cyclotron orbit while the ion-of-interest remains mostly un-excited. To boost the performance in both resolution and the required time, the contaminants are excited with a dipolar RF field employing Ramsey's method of time-separated oscillatory fields technique [31]. Here, a short RF pulse (with constant amplitude) is applied. This pulse is followed by a waiting period and after a pulse with same duration is applied again. It is important to preserve phase coherence for the both RF-on periods.

This method is relatively fast and typically less than 100 ms in total for the excitation procedure is needed to resolve ions having about 1 Hz cyclotron frequency difference. The ions of interest are allowed to gain some cyclotron motion in the excitation process since the ion bunch is sent back to the purification trap for recooling and recentering. On the way the contaminants hit the 2 mm electrode and thus will be completely removed. Once the ions have been properly re-centered in the purification trap, they are sent back to precision trap for mass measurements or further downstream for decay spectroscopy experiments.

The state-of-the-art example of the purification process is the separation of the isomer in ^{133}Xe at 233 keV, corresponding to 1.7 Hz cyclotron frequency

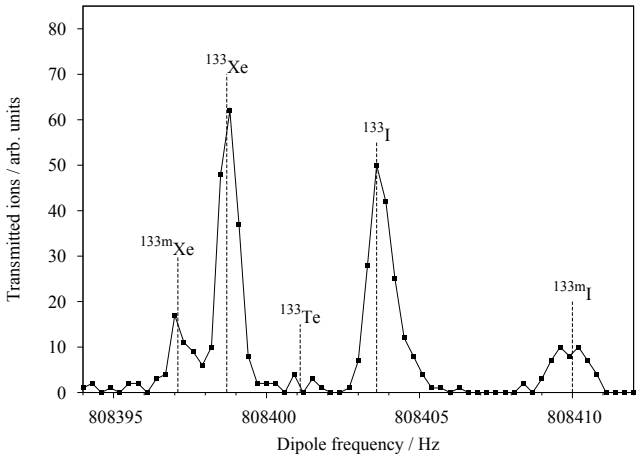

Fig. 8 Dipole frequency scan near the ν_+ frequency of ^{133}Xe using 20/40/20 ms On/Off/On pattern for dipolar RF field. The two states of xenon are clearly separated. Other isotopes are also present due to low resolving power of the purification trap. Resolving power $M/\Delta M \approx 10^6$ is reached.

difference at JYFLTRAP [40]. Here only 60 ms was used for the excitation process in the precision trap and all in all about 500 ms was needed to prepare a monoisomeric bunch of ^{133m}Xe ions. A dipolar frequency scan in the precision trap shown in Fig. 8 showing the transmission of different ion species.

Without this cleaning method several experiments would have not been possible. Like the Q-value measurements of ^{54}Co and ^{50}Mn [41] which both have half-lives less than 300 ms. Other methods would have required a great deal of more time to separate the states [42].

5.2 Time-of-flight ion-cyclotron resonance measurement

Here the steps required to perform high-precision cyclotron frequency measurement using time-of-flight ion-cyclotron (TOF-ICR) [29, 30] are explained.

5.2.1 Magnetron excitation

The first step after capturing the monoisomeric bunch of ions to the precision trap is the magnetron radius expansion. This is done with a short dipole RF pulse at magnetron frequency of 170 Hz. It is important that the magnetron radius expansion prior to the quadrupolar excitation is the same for all ions, and more importantly, for all ion bunches. In order to eliminate bunch-to-bunch variations, the phase of the dipole rf field is fixed to the injection time of the ions [43]. This is called *magnetron phase locking*. Fig. 9 shows a scan where the time between the ion injection and the start of the dipolar excitation has been varied. After dipolar excitation, the quadrupolar excitation is switched

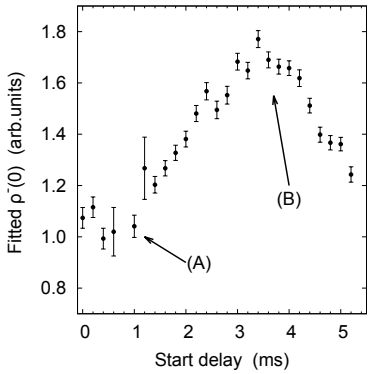

Fig. 9 A magnetron phase-locking scan. The starting time of the dipolar excitation time scanned. On the vertical axis the magnetron orbit radius after RF dipolar excitation ($\rho^-(0)$) is plotted. The radius is obtained from fits to the resonance curves (see Fig. 10 where resonances corresponding to delay times A and B are shown). The period of the magnetron motion is $\approx \frac{1}{170\ \mathrm{Hz}} \approx 5.9$ ms

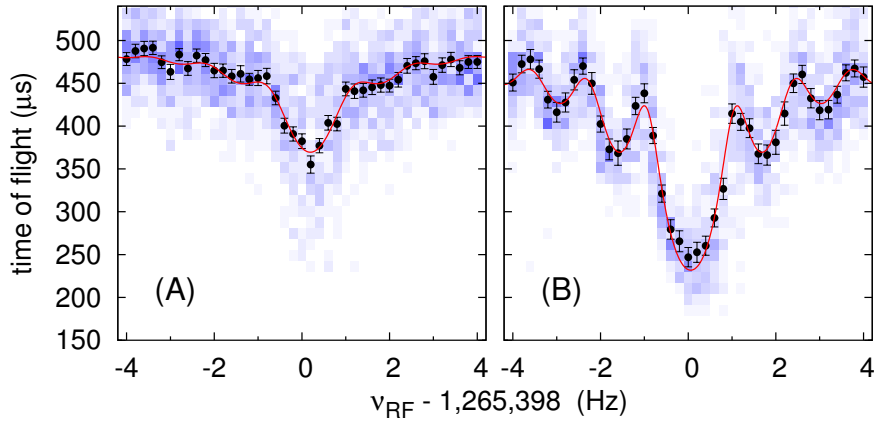

Fig. 10 (Color online) The TOF-ICR curves obtained with magnetron excitation start delays marked in Fig. 9 with (A) and (B). The resonance curve will be deeper when the initial magnetron radius ($\rho^-(0)$) is larger.

on to convert the induced magnetron motion to cyclotron motion. Two TOF-ICR curves are shown in Fig. 10. One with a delay time of 0.6 ms (marked with A) and one with 3.6 ms (marked with B). For case A, the excitation is in the opposite phase to the magnetron motion of the ions, and for case B they are in the same phase.

Thus, to ensure similar magnetron radii for all ion bunches it is important to lock the phase of the excitation. Its absolute value is less important, since a larger resonance effect can be accomplished by increasing the amplitude of the driving RF generator.

5.2.2 Quadrupolar excitation

After the magnetron excitation, the quadrupole excitation is switched on to mass-selectively convert the magnetron motion to cyclotron motion. The excitation duration T_{RF} and the quadrupole RF field amplitude V_{RF} are tuned so that one conversion from magnetron to cyclotron happens only at the resonance frequency $\nu_+ + \nu_-$. With other frequencies the conversion is only partial. The quadrupole RF field frequency (ν_{RF}) is scanned over an interval including the cyclotron frequency ν_c of the ions.

6 Complete atomic mass measurement procedure

Penning trap mass spectrometry provides cyclotron frequency ratios between the ions of interest and the reference ions. The frequency ratio is converted to a mass ratio using Eq. (2). By using a reference with a well-known atomic mass, the mass of the ions of interest can be obtained precisely. The determination of frequency ratios is explained in the following.

6.1 Measurement pattern

An ion bunch goes through the following steps:

1. Accumulation in the RFQ
2. Purification in the purification trap
3. High-resolution cleaning in the precision trap (if needed)
4. Re-cooling and re-centering in the purification trap
5. Ion excitations in the precision trap with quadrupole RF field
6. TOF recording

These steps are repeated for subsequent bunches using different quadrupolar excitation frequencies ν_{RF}. The full procedure is shown in Fig. 11. To maximize the efficiency, the RFQ and the Penning traps are operated in parallel, thus minimizing the measurement time needed. Once enough data is accumulated for the reference ions, the measurement is switched over to the ion species of interest. When enough data is obtained for the ions of interest, the reference ions are scanned again. This procedure is repeated as long as needed.

6.2 Interleaved scanning

The production rate for the ions of interest can be very poor so that most cycles have no detected ions. It may take several hours to gather sufficient statistics for data analysis. Thus, the time between two reference measurements will be long, and changes in the trap environment may cause shifts in the resonance frequency. The conditions of the measurements will be more similar when they are performed in almost parallel fashion.

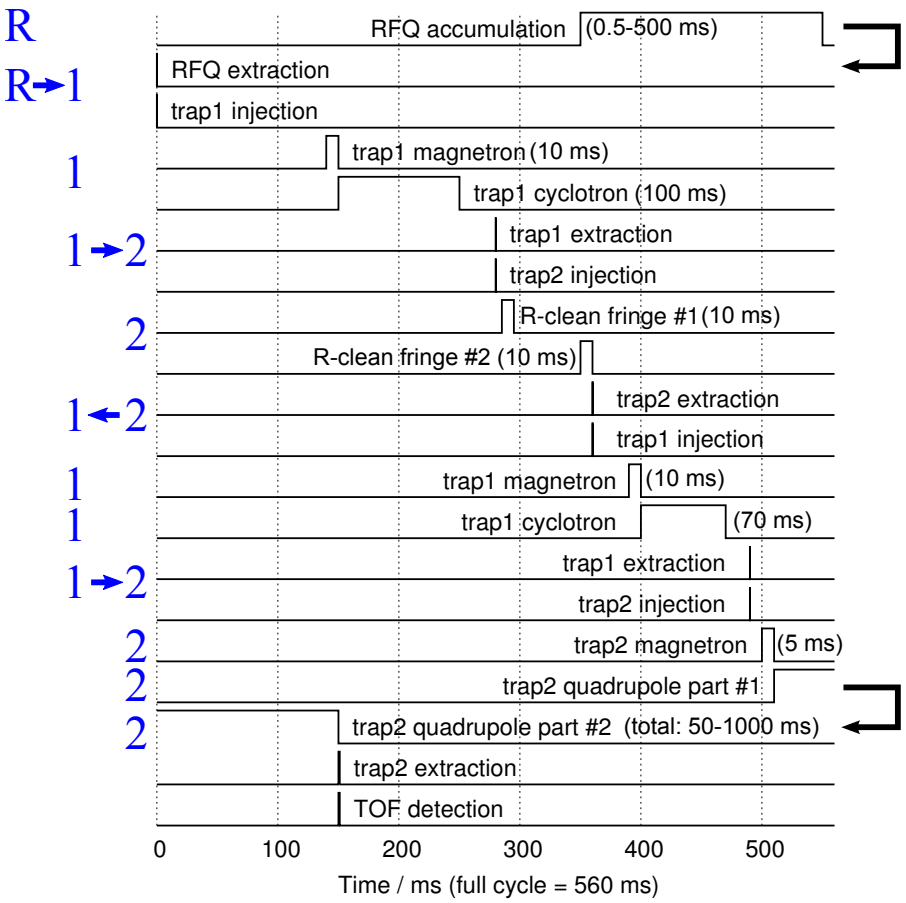

Fig. 11 (Color online) A typical timing pattern used. The blue letters on the left show the location of the ions: R = RFQ, 1 = purification trap, 2 = precision trap. The arrow indicates the transfer of the ions between the traps. From ions' point of view the steps happen from the first row downwards. It should be noted that each of the traps (RFQ, purification and precision) are run in parallel. The arrows on the right depict the start of the next timing cycle.

Switching between two ion species is a simple operation during the measurements. The parameters requiring a change are limited to the following ones:

- mass-dependent parameters, such as:
  - IGISOL separator magnet
  - transportation time from the cooler to the purification trap
  - transportation time from the purification trap to the precision trap
  - the purification trap cyclotron frequency
- production-rate-dependent beam gate timing
- Ramsey-cleaning parameters (if applicable)

Except for the separator magnet, the changes can be performed in less than a second. Changing IGISOL dipole separator magnet to transmit another mass number may take up to 15 seconds. Thus, it is not practical to change between the ion species after every measurement cycle (0.2–5 sec). A measurement program, which switches between two ion species after one or more fully completed frequency sweeps (0.5–2 min), has been developed.

7 Trap performance and systematic studies

The trap performance has been extensively studied. Fluctuations and inhomogeneity of the magnetic field as well as mass-dependent and residual systematic errors related to JYFLTRAP have been investigated. In this section, different optimization procedures are described and systematic uncertainties quantified.

7.1 Magnetic field fluctuations

Although the magnetic field of the superconducting magnet is actively screened, there are some fluctuations in the field. These are mostly caused by the varying temperature of the immediate surroundings of the superconducting magnet and pressure of the liquid helium vessel of the magnet. Some effort has been put into the stabilization of the temperature by covering the high-voltage cage of the trap platform with plastic cover in order to minimize air flow through the setup. Exhaust helium from the magnet cryostat is released to the lab through a differential pressure valve that keeps a small overpressure in the magnet cryostat.

The fluctuations of the magnetic field have been monitored by continuously measuring the cyclotron frequency of the same ion species. For example, Fig. 12 shows the cyclotron frequency of $^{57}Fe^{+}$ ions measured continuously for about 55 hours. The observed fluctuations are mostly due to changes in the magnetic field, but can include other effects.

In frequency ratio (or mass) measurements the linear drifts are taken into account by interpolating the reference scans recorded right before and after the ion of interest. To account for short-term fluctuations, a long frequency scan such as shown in Fig. 12 is subdivided to 22 min files. A real measurement process is simulated by taking three consecutive files, the first and the third for reference and the intermediate one for the ion of interest. A frequency value is interpolated from the references and compared to the measured value in order to obtain the offset $B - B_{\mathrm{int}}$. The whole 55 hours of data are treated like this, and a distribution of offsets is obtained. Next, the data interval is increased to 44 minutes and so on. Finally, the standard deviations of the different distributions as a function of time interval are obtained as shown in Fig. 13, where a line is fitted through the points.

In the absence of non-linear drifts, the distributions should be constant and correspond to the statistical uncertainty of the individual TOF-ICR curve fits.

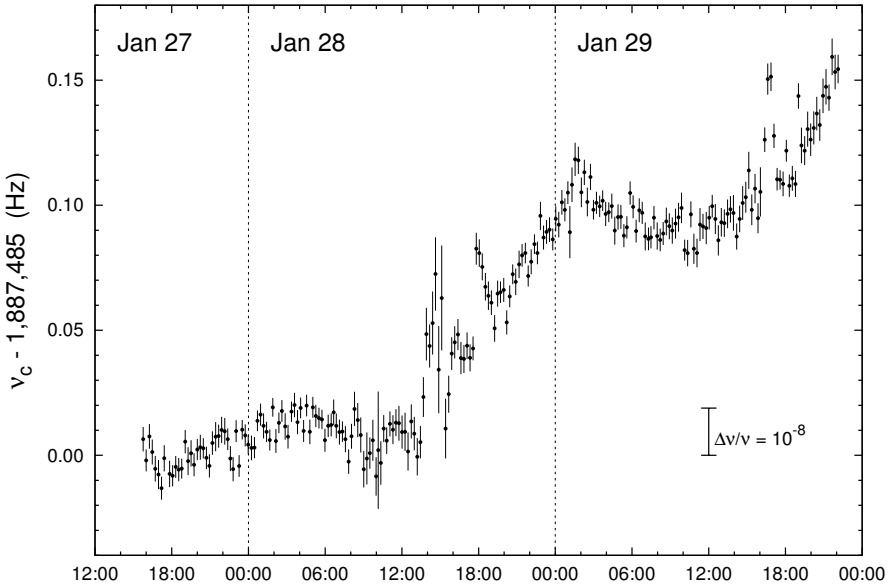

Fig. 12 Cyclotron frequencies of $^{57}Fe^{+}$ ions measured continuously for about 55 hours in January 2009. Every datapoint consist of 22 minutes of collected data. Statistical uncertainty is about 3×10^{-9} for each point. The fluctuations around 14:00-18:00 in January 28 were due to an opening of the entrance doors to outside in the experimental hall (temperature outside was about -5 C). The origin of the frequency deviation around 17:00 in January 29 is not known.

With non-linear drifts present, a positive slope is expected. The y axis crossing resembles the statistical uncertainty of the individual fits. The data shown in Fig. 13 are from January 2009. A similar measurement was done prior to the quenching of the superconducting magnet in 2007 and reported in Ref. [44]. That time the slope was $3.2(2) \times 10^{-11}$ min^{-1}, slightly larger than in 2009. To be on the conservative side, this larger value has been used in all JYFLTRAP measurements.

Non-linear drifts of the magnetic field at JYFLTRAP is a factor of two smaller than the ones reported from ISOLTRAP in 2003 [45] (since 2008 their magnet has been stablized to level beyond their measurement sensitivity [46]). Compared to TRIGATRAP, their fluctuations are a factor of two higher than JYFLTRAP [47]. Non-linear drifts at SHIPTRAP were almost 20-fold worse than at JYFLTRAP but with their recent implementation of pressure and temperature stabilization system their fluctuations have set a record-low value of 0.13×10^{-11} min^{-1} [48]. LEBIT trap has implemented an additional coil to counter the field decay due to the magnet; the remaining non-linear fluctuations are of the order of 0.83×10^{-11} min^{-1} [11] and Canadian Penning trap reports 1.3×10^{-11} min^{-1} [49].

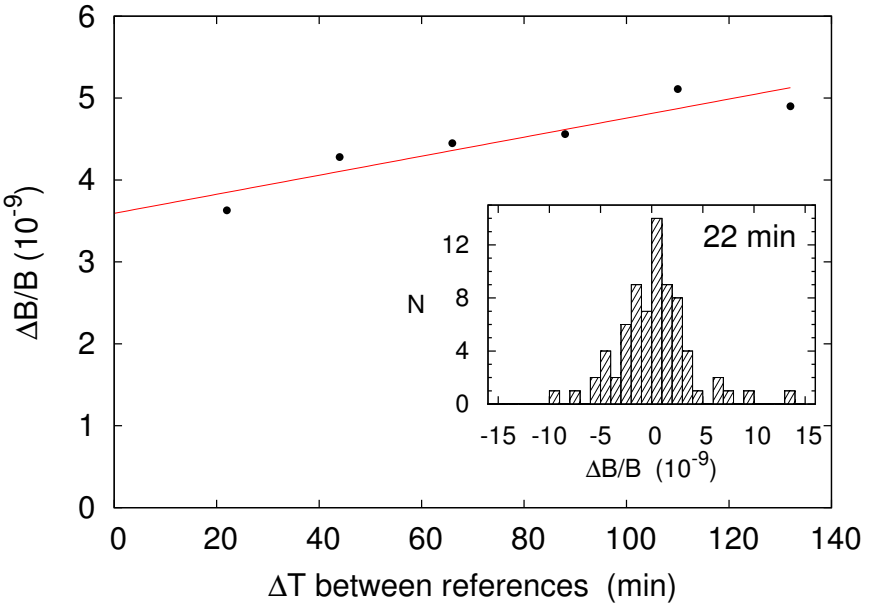

Fig. 13 The standard deviations obtained for different time durations between two consecutive reference scans. A slope of $1.2(2) \times 10^{-11}$ min^{-1} and y-axis crossing of $3.6(2) \times 10^{-9}$ are obtained. The inset shows the distribution of offsets for the first point (22 min). This figure is from Ref. [44].

If a measurement does not exceed 30 minutes at JYFLTRAP, the contribution from non-linear magnetic field drifts are below 1×10^{-9} level. Since the shifts have no preferred direction, contribution from the magnetic field fluctuations are added to the statistical uncertainty.

7.2 Magnetic and electric field inhomogeneities

To minimize the effects of inhomogeneities of the magnetic field the volume in which the ions are confined should be as small as possible. Radially some expansion is needed for the TOF-ICR technique to work, but the amplitude of the axial motion should be minimized. Higher amplitudes result in the ions probing a larger extent of the magnetic field, especially in axial direction, where they are confined only by the electric potential. The axial extent can be minimized by optimizing the ion transfer time between the traps. With a non-optimal transfer time the ions gain energy in the transfer process. This can be observed not only as a shorter time of flight of the ions when extracted from the trap but also in shifts of the measured cyclotron frequency. In Fig. 14, the cyclotron frequency as a function of the transfer time is shown. With non-optimal times the frequency increases, indicating that the magnetic field is on

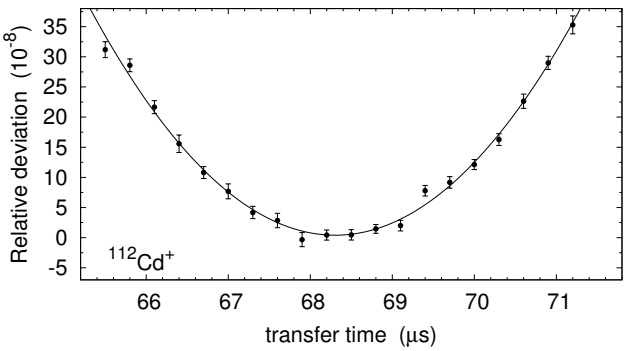

Fig. 14 Measured cyclotron frequency as a function of the transfer time. Here, the transfer time is the time difference between the lowering of the extraction side potential wall of the purification trap and the rising of the injection side potential wall of the precision trap. The frequency is at minimum at the optimum transfer time of 68.3 μs (for $A/q = 112$ ions). TOF-ICR curve fitting also indicates higher energy gain with non-optimal transfer time.

average weaker at the center. This coincides with the shimming data of the magnet: The field was measured to be stronger on both sides of the center of the precision trap.

Both electric and mangetic field inhomogenities could well be minimized by following procedure described in [50]. Especially the electric field optimization will be performed in the new JYFLTRAP setup.

7.3 Carbon clusters cross reference measurements

7.3.1 Background

Mass measurements aim for better and better accuracies. As always in experimental science, this requires better understanding of the measurement instrument. A detailed description of the device and its features has been given in the previous sections. In addition to this, also better, more accurate reference-mass ions are needed for more accurate mass measurements with Penning traps. Since the atomic mass unit (u) is defined as

$$1\mathrm{u} = \frac{1}{12} m\left(^{12}\mathrm{C}\right), \tag{7}$$

the carbon atom or a multiple of carbon atoms, so-called carbon cluster, is an ideal reference mass ion. Carbon clusters are available in equidistant steps of 12 mass units practically covering the whole chart of nuclei. Therefore, carbon clusters are typically used both for systematic studies of the mass spectrometer and also as reference masses.

To study the performance of Penning trap devices, a carbon-cluster ion source based on laser ablation has been used already at ISOLTRAP [45], at

SHIPTRAP [51] and at TRIGA-Trap [47] to quantify mass-dependent systematic effects.

The effort to build a carbon-cluster ion source for JYFLTRAP started around 2005. The first carbon-cluster ions were fired through the trap setup using the first version of the ion source described in Ref. [52]. The ions were produced in a setup situated in an extension of the 90° cross chamber between the RFQ and Penning traps. The setup was closely related to the SHIPTRAP and ISOLTRAP setups. The main difference to JYFLTRAP was the production of ions at the 30 kV high-voltage platform where the ion source was installed.

This place for the source had some clear advantages: the source could be built inside the same 30 kV platform without having a separate high-voltage installation. Also, switching between the carbon cluster source and the main IGISOL source would be easy by simply pulsing the electrodes of the quadrupole bender. Unfortunately, a good beam quality could not be achieved. The energy spread of the ions was far bigger than the depth of the purification trap (100 V) and carbon cluster ions of broad mass range were captured into the trap. Although this version of the cluster ion source could be used for some tests, it was decided to relocate the source further upstream of the RFQ or even before the IGISOL dipole magnet. This would allow an ideal, cooled reference ion beam identical to the beam of the ions of interest from IGISOL.

The ideal place for the carbon-cluster ion source would have been in the IGISOL cave in place of the main ion source. Here, the 55° dipole magnet could have been used to sieve only the cluster species with certain mass to charge ratio. Due to the fact that the IGISOL is almost in constant use by other experiments, this was not feasible. Finally, the ion source was built inside the electrostatic switchyard (at the focal plane of the IGISOL dipole separator magnet), situated on ground potential, see Figs. 1 and 15. At the time there was only an electrostatic bender and a deflector unit inside the switchyard. Even without the full mass separation of the IGISOL dipole magnet, at least the modest mass-selectivity of the RFQ cooler buncher could be used.

7.3.2 Carbon-cluster ion source

In short, the source consists of a carbon plate which is impinged by intense enough laser pulses that some clusters of carbon are evaporated and ionised. The created ions are guided and accelerated with a set of electrodes to create a (bunched) beam. Here, a Q-switched Quantel Brilliant Nd:YAG 532 nm laser was used to create carbon ions from a Sigradur® glassy carbon plate. The laser operates at up to 10 Hz repetition rates. The laser spot is focused down to smaller than 1 mm diameter to achieve high enough energy densities for ablation. The carbon plate is situated on a rotating disk to ensure that the laser does not burn a hole through the plate. See Fig. 15. A more thorough description of the carbon-cluster ion source can be found in Refs. [52, 53].

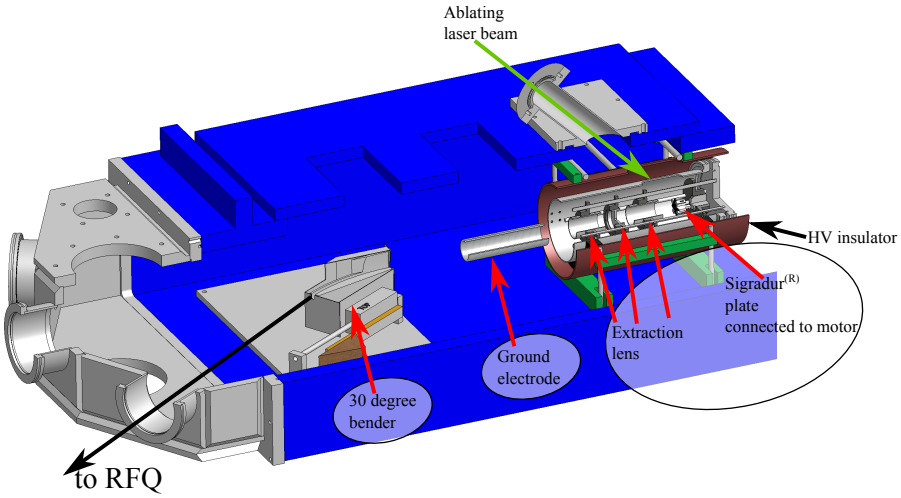

Fig. 15 (Color online) A cut-view of the carbon cluster ion source located at the electrostatic switchyard. The carbon plate at 30 kV of potential and extraction electrodes are housed within a high voltage insulator. The laser pulses hit the Sigradur® plate at 45° angle through a sapphire window on top of the vacuum chamber. The clusters are accelerated to $30q$ keV of energy, deflected by 30° with an electrostic beam deflector to the JYFLTRAP beamline for the injection to the RFQ.

7.3.3 Measurements and results

The cross-reference measurements were performed to quantify the mass-dependent frequency shifts. Since the mass ratios of carbon clusters are known, the shifts in frequency ratios can be quantified. In total more than 200 cyclotron frequency ratios were obtained. Three different sized cluster ions ($^{12}C_7^+$, $^{12}C_{10}^+$ and $^{12}C_{13}^+$) were chosen as reference masses. These were measured against five to eight different sized clusters. To achieve better precision in determining the centre frequency, Ramsey excitation schemes were used. A full description of the measurement parameters can be found in Ref. [53].

Two main systematic properties of the JYFLTRAP setup were quantified: the mass-dependent uncertainty and the so-called residual uncertainty. The mass-dependent uncertainty estimates the relative frequency shift due to the difference in mass between the reference ion and the ion of interest. The residual uncertainty contains all the remaining systematic uncertainties of the setup.

The mass dependent uncertainty was measured to be

$$\sigma_m(r)/r = 7.8(3) \times 10^{-10} \times \frac{\Delta m[\mathrm{u}]}{\mathrm{u}} \tag{8}$$

and the residual uncertainty

$$\sigma_{res}(r)/r = 1.2 \times 10^{-8}, \tag{9}$$

where r is the measured cyclotron frequency ratio. With $\Delta m \leq 24$u – which is the case with all JYFLTRAP mass measurements performed so far – the uncertainties are

$$\sigma_m(r)/r = 7.5(4) \times 10^{-10} \times \frac{\Delta m[\mathrm{u}]}{\mathrm{u}} \tag{10}$$

$$\sigma_{res}(r)/r = 7.9 \times 10^{-9}. \tag{11}$$

7.3.4 Future of carbon clusters at JYFLTRAP

The carbon-cluster ion source that has been built and used for the systematic studies of the JYFLTRAP setup worked very well. Because it has to be manually removed from the beam line to inject beam from IGISOL into the trap, it was never used as a reference ion source. Building the high-voltage platform inside a vacuum chamber which was on ground potential was not ideal. If the usual 30 kV potential was used, occasional sparks occurred between the platform and the ground potential. This was circumvented by using a slightly lowered high-voltage than normal. This had no effect on the final systematic measurements and results.

Now that the whole IGISOL setup is moving to a different location, the systematic measurements should be at least partly repeated to confirm the good operation of JYFLTRAP. It is also a great opportunity to improve the cluster ion source itself.

A tentative location for the carbon-cluster ion source in the future is a separate off-line ion source station, located so that the mass-selection power of the dipole magnet could be used.

7.4 Mass doublets

Frequency ratio measurements of ions with same A/q ratio form a special class of JYFLTRAP measurements. Although frequency shifts due to electric field imperfections and tilt between electric and magnetic fields axis are present [54], the effect in the frequency ratio is negligible compared to statistical uncertainty.

Several mass doublet measurements have been done at JYFLTRAP. Mostly these are Q-value measurements of superallowed beta emitters [55] and of rare weak decays (see e.g. [56, 57]). In these measurements no residual systematic uncertainty as described in the previous section has been added, and precisions in the 10^{-9} range have been achieved. The mass differences of several mass doublets that are known to very high precision have been measured to check the reliability. These include $^{26}\mathrm{Al}^m$ with ^{26}Al as reference, $^{34}\mathrm{Cl}^m$ with ^{34}Cl as reference and ^{76}Ge with ^{76}Se as reference [23, 58].

Doublet measurement technique gives a significant boost compared to "ordinary" mass measurements. In Fig. 16 precisions obtained for superallowed β emitter ^{38}Ca in three trap facilities are given. In addition to JYFLTRAP,

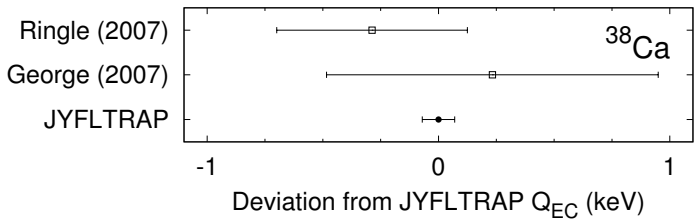

Fig. 16 Comparison of Q values obtained with different trap setups. All results are in perfect agreement. JYFLTRAP measurement was performed as mass doublets while the other two measurements determined only the mass of the parent.

the Q value was measured at ISOLTRAP (George 2007 [34]) and at LEBIT (Ringle 2007 [59]). Their measurements concentrated only on ^{38}Ca mass; mass of the daughter, ^{38m}K, was taken from literature. LEBIT measurement was performed with doubly charged ions while ISOLTRAP measurement relied on Ramsey method. As seen, the JYFLTRAP result is at least 5 times more precise. Recently the doublet technique has been utilized at SHIPTRAP to measure Q values of double-electron capture candidates (see e.g. [60, 61]).

7.5 Present performance and limits

In terms of IGISOL production yields, the most exotic species so far measured are neutron rich nuclei such as ^{122}Pd, ^{114}Tc and ^{103}Y. Their yield was less than 1 ion/s and half-lives about 100 ms [62].

The narrowest peak width achieved with the purification trap has been about 10 Hz ($\Delta\nu_{FWHM}$), which corresponds to mass resolving power $R = M/\Delta M$ for singly charged $A = 100$ ions of about 10^5. With moderate mass resolving power ($\approx 10^4$) the transmission of the whole RFQ and trap line has been about 40 %. This was measured using ^{62}Ga ions by measuring their decay rate with a silicon detector before the RFQ and after the Penning trap.

With the high-resolution cleaning method the best achieved so far is 1 Hz which corresponds to $R = 10^6$ for $A = 100$ ions. The transmission when using high-resolution cleaning method is very low; about 30 ions/bunch was demonstrated in Ref. [40] although yield from IGISOL would have allowed much larger bunch sizes. Here the limiting factor is space charge in the precision trap.

8 Data analysis procedure

The recorded TOF-ICR data consist of the time-of-flight of the ions as a function of the frequency of the exciting RF field. The lineshape of the resonance curve is well described in Ref. [30] for a rectangular excitation amplitude shape and in Ref. [63] for time-separated oscillatory fields. Many aspects of the data

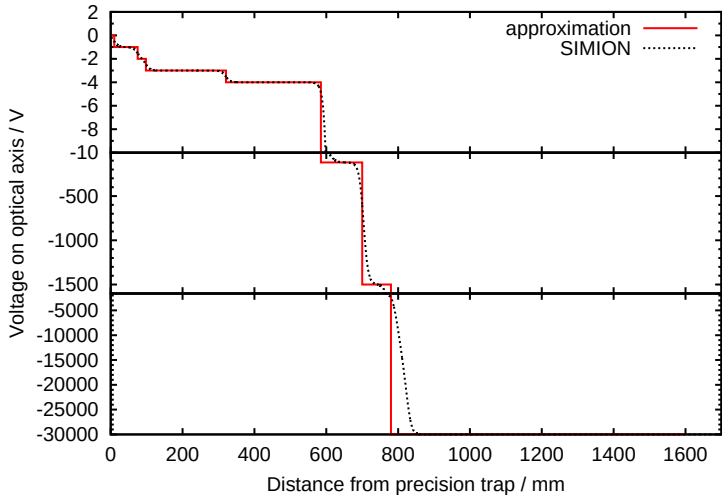

Fig. 17 (Color online) Comparison of the realistic (from SIMION) and the approximated electric potentials. The zero-potential is chosen to be the potential of the ring electrode of the precision trap. The earth-ground in this scale is then at −30 kV. The MCP detector is located about 1600 mm away from the precision trap. The approximation reproduces the most crucial low voltage part at 0–600 mm very well.

analysis procedure have been elaborated at ISOLTRAP (see e.g. [45]). More details about data analysis procedures at JYFLTRAP can be found in Ref. [64].

8.1 Theoretical TOF determination

After quadrupolar excitation in the precision trap (as described in chapter 5.2.2) the extraction side potential wall of the trap is lowered and the ions are ejected towards the MCP detector, which is located at ground potential, about 1.6 m downstream from the precision trap (see also Fig. 1). The time-of-flight can be calculated since the magnitudes of the electric and magnetic fields are known from simulations. The electric potential along the geometry axis is shown in Fig. 17, and the magnetic field in Fig. 18. The fields are extracted from the ion optics simulation program SIMION, which gives the field values along the flight path with grid size of 1 mm. To make this less computer power demanding the fields are averaged over sections which can be described either with a constant number or, at most, with a second order polynomial. The full time-of-flight can then be calculated with Eq. (5).

It is important to extract the ions slowly over the magnetic field gradient so that ions with more radial energy will gain significantly more axial energy when crossing the field gradient. At $\approx$ 600 mm the ions are electrostatically significantly accelerated. At this point the magnetic field is only about 0.1 T. The ions are then hitting the MCP detector with $30q$ keV of energy.

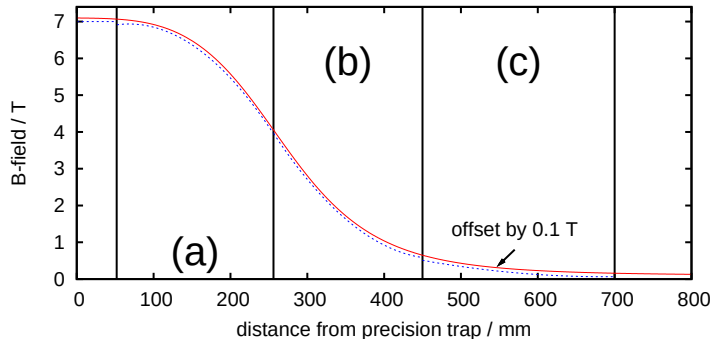

Fig. 18 (Color online) Comparison of the realistic and the approximated magnetic fields. The field is split in five parts, where two sections have constant 7 T and 0 T and the three sections marked (a-c) in between are well described with second order polynomial functions (dashed blue line). The realistic field shape from SIMION (solid red line) is offset by 0.1 T for clarity.

8.2 Determination of the experimental TOF and its uncertainty

Several bunches of ions are recorded for each frequency. A TOF gate is applied so that only ions within a certain TOF interval are accepted. The gate has to be set so that no ions of interest are left out. This is illustrated in Fig. 19, where the TOF gate has been set to be 155–330 μs (depicted with full vertical bars). Ions outside the gate do not contribute to the cyclotron frequency determination. Another gate is imposed by the number of detected ions. Typically, the analysis is performed by dividing the data into classes according to how many ions were detected in a single bunch. This is called countrate class analysis and is well described in Ref. [45]. This way, the fitted frequency can be extracted as a function of detected ions per bunch. If contaminants are present, the frequency is expected to shift with increasing number of ions.

To calculate the TOF uncertainty at each frequency a so-called mean-corrected sum-statistics method is used in order to provide uncertainty even for the frequencies where only few ions were detected. In these cases ordinary standard deviation of the mean value would produce unrealistic uncertainties [64]. First, the mean TOF for each frequency point is calculated. Then, the distributions of each frequency are stacked together keeping the mean value as a central value. The standard deviation (σ) of such a distribution is

$$\sigma\left(\overline{T}\right) = \sqrt{\frac{\sum_{m=1}^{M}\left[\sum_{n=1}^{N_m}\left(\overline{T}_m - T_{m,n}\right)^2\right]}{N-1}}, \tag{12}$$

where the inner sum is over all ions (N_m) excited with frequency ν_m. $T_{m,n}$ is the TOF of one ion and $\overline{T}_m$ is their mean TOF. The outer sum is over all excitation frequencies ν_m. The total number of ions is $N = \sum_m N_m$.

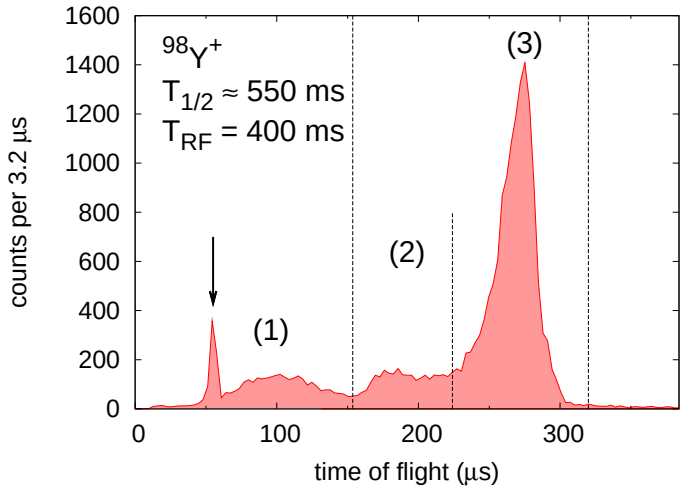

Fig. 19 (Color online) A typical time-of-flight spectrum of short-living β^- decaying ions consisting of all ions regardless of excitation frequency in the trap. The peaks at (2) and (3) mark the ions excited with $\nu_{\mathrm{RF}} \approx \nu_c$ and $\nu_{\mathrm{RF}} \neq \nu_c$, respectively. The peak (1) consists of doubly-charged β^--decay daughter ions. Their time of flight is short not only because they are doubly charged but also due to recoil energy gained in the decay process. The sharp peak marked with arrow consists of He^+ ions, formed in collisions of β decay recoils with residual gas atoms. Only the ions detected between the two dashed vertical bars are used for TOF determination. Naturally all detected ions are used for the count-rate-class analysis.

For each frequency the standard deviation of the mean is obtained as

$$\sigma\left(\overline{T_k}\right) = \frac{\sigma\left(\overline{T}\right)}{\sqrt{N_k}}, \tag{13}$$

where N_k is the number of ions detected at that frequency.

8.3 Cyclotron frequency ratio determination

The ion-of-interest scans have been obtained consecutively or interleaved as described in section 6.2. The TOF-ICR curves are fitted using the countrate class analysis (see Ref. [45]) to account for shifts due to contaminating ions. At JYFLTRAP, the MCP efficiency was measured to be about 60% [65] thus, in order to get a frequency value corresponding to one stored ion in the trap, the countrate classed results were extrapolated to a value of 0.6.

With consecutive scanning, where the ion species is switched every 30 minutes or more, the reference frequency needs to be interpolated from adjacent scans to the ion-of-interest scan. From the interpolated frequency and the ion-of-interest frequency the final cyclotron frequency ratio is obtained.

For a single measurement consisting of a reference scan (at time t_0 having frequency ν_0), an ion-of-interest scan (at time t_1 having frequency ν_{meas}) and

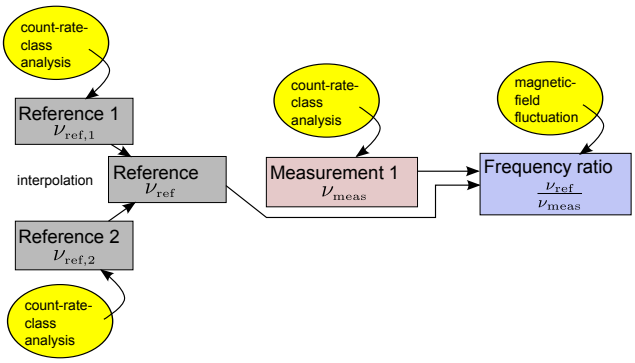

Fig. 20 Determination of a single frequency ratio using two reference ion scans and an ion-of-interest scan. The countrate class analysis is performed for each scan. Uncertainty due to the magnetic field fluctuation is added to frequency ratio.

a reference scan again (at t_2 with ν_2), the interpolated reference ion frequency ν_{ref} at the time of ν_{meas} is

$$\nu_{\mathrm{ref}} = \frac{1}{t_2 - t_0}\left[\nu_0\,(t_2 - t_1) + \nu_2\,(t_1 - t_0)\right] \tag{14}$$

with uncertainty $\sigma(\nu_{\mathrm{ref}})$

$$\sigma(\nu_{\mathrm{ref}}) = \frac{1}{t_2 - t_0}\sqrt{(t_2 - t_1)^2\,\sigma(\nu_0)^2 + (t_1 - t_0)^2\,\sigma(\nu_2)^2}. \tag{15}$$

After having both the interpolated reference frequency (ν_{ref}) and the frequency of the ion of interest (ν_{meas}), the frequency ratio r is

$$r = \frac{\nu_{\mathrm{ref}}}{\nu_{\mathrm{meas}}} \tag{16}$$

with uncertainty

$$\sigma(r) = r\sqrt{\left(\frac{\sigma(\nu_{\mathrm{ref}})}{\nu_{\mathrm{ref}}}\right)^2 + \left(\frac{\sigma(\nu_{\mathrm{meas}})}{\nu_{\mathrm{meas}}}\right)^2}. \tag{17}$$

With interleaved scanning no interpolation is needed. Uncertainty due to magnetic field fluctuation is quadratically added to the frequency ratio uncertainty. The analysis steps are summarized in Fig. 20.

When a chain of data (Ref-Meas-Ref-...-Meas-Ref) has been taken, the final frequency ratio is weighted average of the individual frequency ratios. With interleaved scanning procedure a long measurement is split to convenient chunks that consists usually of about 30 minutes of data. The mass dependent uncertainty and the residual uncertainty are added in this point, as illustrated in Fig. 21. So far any data obtained with JYFLTRAP has not been corrected

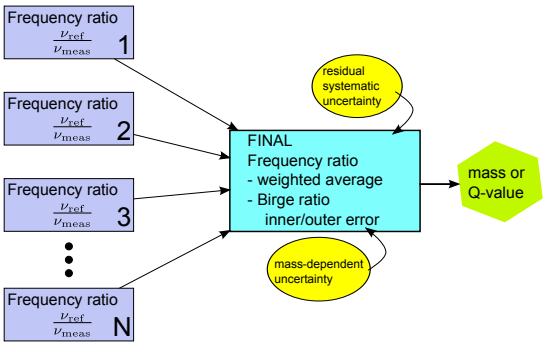

Fig. 21 Determination of the final frequency ratio. Using N individual frequency ratios (as shown in Fig. 20) the final frequency ratio is obtained by calculating the weighted average of the individual values. The inner and outer errors are calculated. The mass dependent and residual systematic uncertainty are added at the very end.

with mass dependent shift. Instead, this shift is added as an uncertainty. Additionally the Birge ratio [66] needs to be calculated. For this, both the inner error

$$\sigma_{\text{int}}^2 = \frac{1}{\sum_i \frac{1}{\sigma_i^2}} \tag{18}$$

and the outer error

$$\sigma_{\text{ext}}^2 = \frac{\sum_i \frac{1}{\sigma_i^2} (r_i - \overline{r})^2}{(n-1) \sum_i \frac{1}{\sigma_i^2}} \tag{19}$$

are needed (r_i are the individual frequency ratios and the Birge ratio is $R = \sigma_{\text{ext}}/\sigma_{\text{int}}$ [66]. If both the inner and the outer errors are about equal, the fluctuation around the mean value is purely statistical. Common practise has been that if either of the error is larger, then the larger one is used as the final error. At this stage the mass dependent and residual systematic uncertainties are added (see Fig. 21).

8.4 Mass and Q-value

Finally the atomic mass of the ion of interest m_{meas} is obtained (for singly charged ions and omitting binding energies of the missing electrons)

$$m_{\text{meas}} = r \times (m_{\text{ref}} - m_e) + m_e, \tag{20}$$

where m_e is mass of an electron. Mass uncertainty is

$$\sigma\left(m_{\text{meas}}\right) = \sqrt{\sigma(r)^2 (m_{\text{ref}} - m_e)^2 + \sigma(m_{\text{ref}})^2 r^2}, \tag{21}$$

where uncertainty of the electron mass as well as binding energies of the missing electrons are neglected.

Mass differences or Q-values are calculated for singly charged ions by using the relation

$$Q = m_{\mathrm{meas}} - m_{\mathrm{ref}} = (r-1)(m_{\mathrm{ref}} - m_e) + \Delta B_e, \tag{22}$$

where ΔB_e term (with singly charged ions typically few eV) arises from the binding energy difference of the missing atomic electrons. The Q value uncertainty is

$$\sigma(Q) = \sqrt{\sigma(r)^2(m_{\mathrm{ref}} - m_e)^2 + \sigma(m_{\mathrm{ref}})^2(r-1)^2}, \tag{23}$$

when neglecting uncertainty of the electron mass and the atomic electron binding energies. Typically contribution from the reference mass uncertainty $\sigma(m_{\mathrm{ref}})$ can also be omitted since for A/q doublets $(r-1) < 10^{-3}$ and thus in most of the cases uncertainty in the Q-value can be simply written as

$$\sigma(Q) \approx \sigma(r) \times (m_{\mathrm{ref}} - m_e). \tag{24}$$

9 Summary of JYFLTRAP atomic mass measurements

The JYFLTRAP Penning trap setup was operational since 2003 until June 2010 when the whole IGISOL facility, including JYFLTRAP, were shut down for relocation. The atomic masses of more than 200 short-living nuclei have been measured and published as summarized in Table 7. Nearly 50 more have been measured which are expected to be published shortly, see Table 8. An up-to-date list of the measured and published nuclei can be found from the JYFLTRAP website [67].

The atomic masses measured at JYFLTRAP are shown in Fig. 22. The main areas of studies are (see for mass measurement references in tables 7 and 8):

- nuclear structure at the n-rich side [68]
- nuclear astrophysics (near ^{58}Ni, rp and νp processes, SnSbTe cycle) [69–72]
- Q-values of superallowed $0^+ \rightarrow 0^+$ β emitters [55]
- Q-values of mirror decays [73]
- testing the Isobaric Mass Multiplet Equation (IMME) [74]
- Q-values of neutrinoless double-electron-capture candidates (2EC) [75]
- Q-values for double-beta decay studies (2β) [76]

All Q-value measurements have measured as doublets and typically precision of better than 1 keV (10^{-8}) have been obtained.

The mass measurement program will be continued as soon as the relocation and upgrade of the IGISOL and JYFLTRAP setups are complete in 2012. Upgrades include, for instance, a new off-line ion source which can be operated independently of the IGISOL frontend, and optional beam ports between the RFQ and Penning traps for adding various devices such as a multi-reflection time-of-flight mass separator.

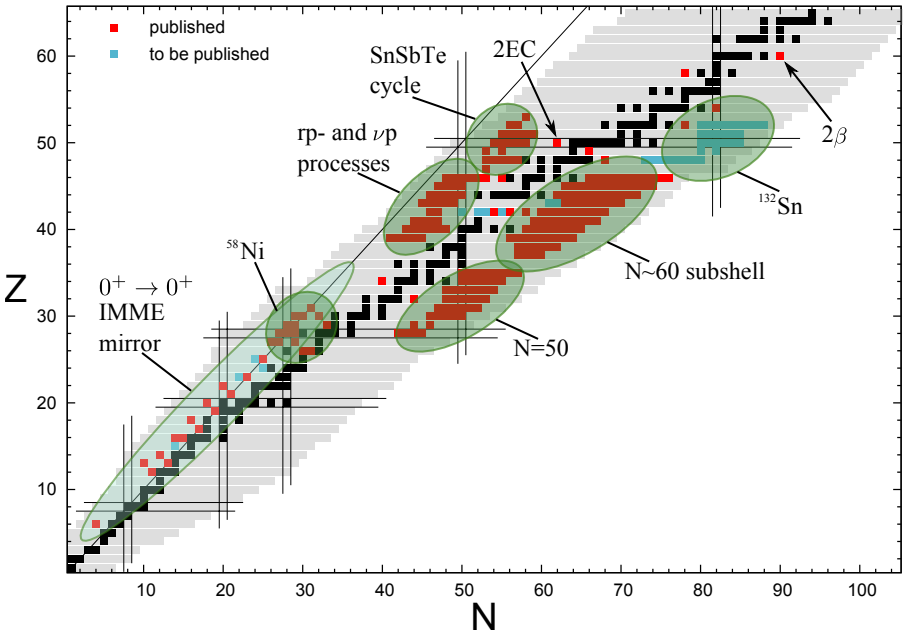

Fig. 22 (Color online) The chart of nuclei where nuclei whose mass has been determined with JYFLTRAP have been indicated. Red symbols indicate published results and light blue the measured ones (see also tables 7 and 8). Also to which studies the measured nuclei contribute have been marked (see text for more explanation).

Acknowledgements This work was has been supported by the European Union (RTD project EXOTRAPS, Contract No. ERBFMGECT980099; RTD project NIPNET, Contract No. HPRI-CT-2001-50034; Fifth Framework Programme "Improving Human Potential-Access to Research Infrastructure", Contract No. HPRI-CT-1999-00044; 6th Framework programme "Integrating Infrastructure Initiative- Transnational Access" Contract No. 506065 (EURONS)) and by the academy of Finland under the Finnish Centre of Excellence Programmes 2000-2005 and 2006-2011.

References

1. H.-J. Kluge, Hyperfine Interact. **196**, 295 (2010).
2. K. Blaum, Phys. Rep. **425**, 1 (2006).
3. I. Bergström *et al.*, Nucl. Instrum. Methods in Phys. Res., Sect. A **487**, 618 (2002).
4. M. Redshaw, J. McDaniel, and E. G. Myers, Phys. Rev. Lett. **100**, 093002 (2008).
5. R. S. Van Dyck *et al.*, Phys. Rev. Lett. **92**, 220802 (2004).
6. C. Diehl *et al.*, Hyperfine Interact. **199**, 291 (2011).
7. G. Gabrielse, Int. J. Mass Spectrom. **251**, 273 (2006).
8. M. Hori *et al.*, Nature **475**, 484 (2011).
9. J. Wang *et al.*, Nucl. Phys. A **746**, 651 (2004).
10. M. Mukherjee *et al.*, Eur. Phys. J. A **35**, 1 (2008).
11. R. Ringle *et al.*, Nucl. Instrum. Methods Phys. Res., Sect. A **604**, 536 (2009).
12. V. S. Kolhinen *et al.*, Nucl. Instrum. Methods Phys. Res., Sect. A **600**, 391 (2009).
13. G. Sikler *et al.*, Nucl. Instrum. Methods Phys. Res., Sect. B **204**, 482 (2003).
14. J. Dilling and the TITAN collaboration, Hyperfine Interact. **196**, 21 (2010).

Table 7 List of isotopes whose mass has been measured with JYLFTRAP. References to publications have also been given.

Z	Element	Mass numbers	References
6	C	10	[77]
12	Mg	23	[78]
13	Al	23, 26	[78, 79]
14	Si	26	[80]
16	S	30, 31	[81, 82]
17	Cl	34, 34m	[58]
18	Ar	34	[77]
19	K	38, 38m	[58]
20	Ca	38	[77]
21	Sc	42, 42m	[79]
22	Ti	42	[83]
23	V	46	[79]
25	Mn	50, 50m	[41]
26	Fe	56-57	[84]
27	Co	53, 53m, 56	[41, 84]
28	Ni	55-57, 70-73	[44, 84]
29	Cu	57-58, 62, 73, 75	[44, 79, 84]
30	Zn	59-60, 62, 76-80	[79, 84, 85]
31	Ga	62, 78-83	[79, 85]
32	Ge	76, 80-85	[23, 85]
33	As	81-87	[85]
34	Se	74, 84-89	[57, 85]
35	Br	85-92	[86]
37	Rb	94-97	[86]
38	Sr	95-100	[87]
39	Y	80-84, 95-103	[62, 88–90]
40	Zr	83-88, 98-105	[87–89]
41	Nb	85-88, 100-108	[62, 88, 90]
42	Mo	88-89, 100, 102-111	[23, 62, 87, 89]
43	Tc	88-92, 106-114	[62, 89, 91]
44	Ru	90-94, 106-116	[62, 89, 91]
45	Rh	92-95, 108-119	[62, 89, 91]
46	Pd	94-99, 101, 112-122	[62, 89, 91, 92]
47	Ag	100	[92]
48	Cd	101-105, 116	[92, 93]
49	In	102,104, 115	[92, 94]
50	Sn	104-108, 112	[56, 95]
51	Sb	106-110	[95]
52	Te	108-109, 130	[93, 95]
53	I	111	[95]
54	Xe	136	[96]
58	Ce	136	[96]
60	Nd	150	[97]

15. J. Ketelaer *et al.*, Nucl. Instrum. Methods Phys. Res., Sect. A **594**, 162 (2008).
16. V. S. Kolhinen *et al.*, Nucl. Instrum. Methods Phys. Res., Sect. A **528**, 776 (2004).
17. A. Jokinen *et al.*, Int. J. Mass Spectrom. **251**, 204 (2006).
18. M. Smith *et al.*, Phys. Rev. Lett. **101**, 202501 (2008).
19. M. Block *et al.*, Nature **463**, 785 (2010).
20. J. Äystö, Nucl. Phys. A **693**, 477 (2001).
21. H. Penttilä *et al.*, Eur. Phys. J. A **25**, 745 (2005).
22. P. Karvonen *et al.*, Nucl. Instrum. Methods Phys. Res., Sect. B **266**, 4794 (2008).
23. S. Rahaman *et al.*, Phys. Lett. B **662**, 111 (2008).

Table 8 List of isotopes whose mass has been measured at JYFLTRAP but not yet published.

Z	Element	Mass numbers
15	P	29
24	Cr	49
25	Mn	49
41	Nb	108
42	Mo	92, 94-98, 100
43	Tc	104-105
48	Cd	121-128
49	In	129-131
50	Sn	130-135
51	Sb	131-136
52	Te	130, 132-140

24. A. Nieminen *et al.*, Nucl. Instrum. Methods Phys. Res., Sect. A **469**, 244 (2001).
25. L. S. Brown and G. Gabrielse, Phys. Rev. A **25**, 2423 (1982).
26. G. Gabrielse, Int. J. Mass Spectrom. **279**, 107 (2009).
27. G. Savard *et al.*, Phys. Lett. A **158**, 247 (1991).
28. L. S. Brown and G. Gabrielse, Rev. Mod. Phys. **58**, 233 (1986).
29. G. Gräff, H. Kalinowsky, and J. Traut, Z. Phys. A **297**, 35 (1980).
30. M. König *et al.*, Int. J. Mass Spectrom. **142**, 95 (1995).
31. N. F. Ramsey, Rev. Mod. Phys. **62**, 541 (1990).
32. G. Bollen *et al.*, Nucl. Instrum. Methods Phys. Res., Sect. B **70**, 490 (1992).
33. M. Kretzschmar, Int. J. Mass Spectrom. **264**, 122 (2007).
34. S. George *et al.*, Phys. Rev. Lett. **98**, 162501 (2007).
35. T. Eronen *et al.*, Nucl. Instrum. Methods Phys. Res., Sect. B **266**, 4527 (2008).
36. K. Farrar, Nucl. Instrum. Methods Phys. Res., Sect. A **485**, 780 (2002).
37. G. Gabrielse, L. Haarsma, and S. Rolston, Int. J. Mass Spectrom. Ion Process. **88**, 319 (1989).
38. H. Raimbault-Hartmann *et al.*, Nucl. Instrum. Methods Phys. Res., Sect. B **126**, 378 (1997).
39. M. Eibach *et al.*, Int. J. Mass Spectrom. **303**, 27 (2011).
40. K. Peräjärvi *et al.*, Appl. Radiat. Isot. **68**, 450 (2010).
41. T. Eronen *et al.*, Phys. Rev. Lett. **100**, 132502 (2008).
42. K. Blaum *et al.*, Nucl. Phys. A **752**, 317c (2005).
43. K. Blaum *et al.*, J. Phys. B: At., Mol. Opt. Phys. **36**, 921 (2003).
44. S. Rahaman *et al.*, Eur. Phys. J. A **34**, 5 (2007).
45. A. Kellerbauer *et al.*, Eur. Phys. J. D **22**, 53 (2003).
46. M. Marie-Jeanne *et al.*, Nucl. Instrum. Methods Phys. Res., Sect. A **587**, 464 (2008).
47. J. Ketelaer *et al.*, Eur. Phys. J. D **58**, 47 (2010).
48. C. Droese *et al.*, Nucl. Instrum. Methods Phys. Res., Sect. A **632**, 157 (2011).
49. G. Savard *et al.*, Phys. Rev. Lett. **95**, 102501 (2005).
50. D. Beck *et al.*, Nucl. Instrum. Methods Phys. Res., Sect. A **598**, 635 (2009).
51. A. Chaudhuri *et al.*, Eur. Phys. J. D **45**, 47 (2007).
52. V.-V. Elomaa *et al.*, Nucl. Instrum. Methods Phys. Res., Sect. B **266**, 4425 (2008).
53. V.-V. Elomaa *et al.*, Nucl. Instrum. Methods Phys. Res., Sect. A **612**, 97 (2009).
54. G. Gabrielse, Phys. Rev. Lett. **102**, 172501 (2009).
55. J. C. Hardy and I. S. Towner, Phys. Rev. C **79**, 055502 (2009).
56. S. Rahaman *et al.*, Phys. Rev. Lett. **103**, 042501 (2009).
57. V. S. Kolhinen *et al.*, Phys. Lett. B **684**, 17 (2010).
58. T. Eronen *et al.*, Phys. Rev. Lett. **103**, 252501 (2009).
59. R. Ringle *et al.*, Phys. Rev. C **75**, 055503 (2007).
60. S. Eliseev *et al.*, Phys. Rev. Lett. **106**, 052504 (2011).
61. S. Eliseev *et al.*, Phys. Rev. C **84**, 012501(R) (2011).
62. J. Hakala *et al.*, The European Physical Journal A - Hadrons and Nuclei **47**, 1 (2011).

63. S. George *et al.*, Int. J. Mass Spectrom. **264**, 110 (2007).
64. T. Eronen, Ph.D. thesis, University of Jyväskylä, 2008.
65. H. Penttilä *et al.*, Eur. Phys. J. A **44**, 147 (2010).
66. R. T. Birge, Phys. Rev. **40**, 207 (1932).
67. JYFLTRAP mass database, http://research.jyu.fi/igisol/JYFLTRAP_masses/.
68. A special issue on ultra-accurate mass determination and related topics, edited by L. Schweikhard and G. Bollen, Int. J. Mass Spectrom. **251**, (2006).
69. R. Wallace and S. Woosley, Astrophys. J. Suppl. Ser. **45**, 389 (1981).
70. H. Schatz *et al.*, Phys. Rep. **294**, 167 (1998).
71. B. A. Brown *et al.*, Phys. Rev. C **65**, 045802 (2002).
72. H. Schatz *et al.*, Phys. Rev. Lett. **86**, 3471 (2001).
73. O. Naviliat-Cuncic and N. Severijns, Phys. Rev. Lett. **102**, 142302 (2009).
74. E. P. Wigner, in *Robert A. Welch foundation conference on chemical research*, edited by W. O. Millikan (Houston, Texas, 1957), Vol. 1, p. 67.
75. R. G. Winter, Phys. Rev. **100**, 142 (1955).
76. F. T. Avignone, S. R. Elliott, and J. Engel, Rev. Mod. Phys. **80**, 481 (2008).
77. T. Eronen *et al.*, Phys. Rev. C **83**, 055501 (2011).
78. A. Saastamoinen *et al.*, Phys. Rev. C **80**, 044330 (2009).
79. T. Eronen *et al.*, Phys. Rev. Lett. **97**, 232501 (2006).
80. T. Eronen *et al.*, Phys. Rev. C **79**, 032802 (2009).
81. J. Souin *et al.*, Eur. Phys. J. A **47**, 1 (2011).
82. A. Kankainen *et al.*, Phys. Rev. C **82**, 052501 (2010).
83. T. Kurtukian Nieto *et al.*, Phys. Rev. C **80**, 035502 (2009).
84. A. Kankainen *et al.*, Phys. Rev. C **82**, 034311 (2010).
85. J. Hakala *et al.*, Phys. Rev. Lett. **101**, 052502 (2008).
86. S. Rahaman *et al.*, Eur. Phys. J. A **32**, 87 (2007).
87. U. Hager *et al.*, Phys. Rev. Lett. **96**, 042504 (2006).
88. A. Kankainen *et al.*, Eur. Phys. J. A **29**, 271 (2006).
89. C. Weber *et al.*, Phys. Rev. C **78**, 054310 (2008).
90. U. Hager *et al.*, Nucl. Phys. A **793**, 20 (2007).
91. U. Hager *et al.*, Phys. Rev. C **75**, 064302 (2007).
92. V.-V. Elomaa *et al.*, Eur. Phys. J. A **40**, 1 (2009).
93. S. Rahaman *et al.*, Phys. Lett. B **703**, 412 (2011).
94. J. S. E. Wieslander *et al.*, Phys. Rev. Lett. **103**, 122501 (2009).
95. V.-V. Elomaa *et al.*, Phys. Rev. Lett. **102**, 252501 (2009).
96. V. S. Kolhinen *et al.*, Phys. Lett. B **697**, 116 (2011).
97. V. S. Kolhinen *et al.*, Phys. Rev. C **82**, 022501 (2010).